An optimized Delay Multiply and Sum ultrasonic imaging algorithm based on sparse arrays and parallel computing

Dong Ming [a,b]*, Gong Heng-da [a], Chen Yuan [2], Zhang Guang-ming [c], Cao Xian-gang [1,2], Wan Xiang [1,2]

[a]School of Mechanical Engineering, Xi'an University of Science and Technology, Xi'an 710054, China;
[b]Shaanxi Key Laboratory of Mine Electromechanical Equipment Intelligent Detection and Control, Xi'an 710054, China;
[c]General Engineering Research Institute, School of Engineering, Faculty of Engineering and Technology, Liverpool John Moores University, Byrom Street, L3 3AF, United Kingdom

*Corresponding author: Dong Ming

E-mail: jesunatg@hotmail.com

Abstract

The Total Focusing Method (TFM) focuses pixels using the Delay and Sum (DAS) beamforming technique, which relies solely on the temporal information of the full matrix capturing dataset while ignoring its spatial information, and the image resolution and contrast achievable with TFM are limited. In this work, a parallel sparse delay multiply and sum (PSDMAS) focusing imaging algorithm based on sparse arrays and parallel computing is proposed to improve contrast resolution and imaging efficiency. A sparse array optimization method is applied to reduce the amount of data. A ratio of main-lobe width and side-lobe peak was constructed as the fitness function and a genetic algorithm was used to find the optimal solution for the array arrangement. Delay Multiply and Sum (DMAS) is employed to enhance the spatial coherence and suppress the clutter artifacts. Parallel computing strategies were implemented to improve imaging efficiency. To validate the effectiveness of the algorithm, we processed the full matrix data collected from simulations and experiments using PSDMAS, the imaging results of the PSDMAS provided a considerable improvement in Array Performance Indicator (API), and better lateral spatial resolution was also achieved. The computation time of PSDMAS was reduced by 99.9% compared to conventional DMAS.

Keywords: total focusing method, full matrix capture, delay multiply and sum, sparse array

1 Introduction

Ultrasonic Testing (UT) has become the most widely used non-destructive testing technique due to its high detection sensitivity and harmlessness to human body [1-2]. Improving image quality is a hot research topic in UT [3-5]. Wang et al. [6] proposed an autocorrelation imaging algorithm combines Multipoint Optimal Minimum Entropy Deconvolution Adjusted (MOMEDA) to identify near-surface flaws in CFRP, achieving error values below 5% for defects at different depths. Ming et al. [7] proposed an acoustic field simulation method based on multi-Gaussian beams, which can simulate the focused sound field in multi-layered anisotropic media, significantly improving the ultrasound detection performance. Phased Array Ultrasonic Testing (PAUT) differs from conventional UT in its ability to control the direction of the emitted ultrasonic beam, which has been widely applied in various industries, including the nuclear industry, aerospace, and mechanical manufacturing [8-10]. Thus, enhancing the effectiveness of PAUT has also received increasing attention.

The Delay and Sum (DAS) beamforming method uses Fermat's principle to calculate the ultrasonic travel time from the focus pixel to the array element and extracts the amplitude of the ultrasonic signal for accumulation and imaging [11]. Due to its ease of computation and high efficiency, DAS is widely used in imaging algorithms such as Synthetic Aperture Focusing Technology (SAFT) and Total Focus Method (TFM) [12-13]. However, DAS only utilizes the amplitude information of the signal, resulting in low image contrast and resolution [14].

Lim et al. [15] proposed the Delay Multiply and Sum (DMAS) beamforming algorithm, where the received ultrasonic signals are first time shifted as in the DAS algorithm, then multiplications are introduced before being summed to create a synthetic focal point. The results demonstrated the feasibility and robustness of DMAS in detecting tumors as small as 2 mm in diameter. Due to the weak coherence between noise and strong coherence between signals, DMAS can suppress noise and improve image quality, and has found wide application in medical tumor detection and other fields [16]. Researchers have combined DMAS beamforming with other phased array imaging algorithms to verify the feasibility of DMAS in industrial inspection. Da et al. [17] combined the DMAS with the FMC dataset, taking full advantage of the spatial information, and achieved better noise rejection and image resolution than TFM. Ziksari et al. [18] proposed a modified version of the DMAS beamformer in the coherent compounding, where the Minimum Variance (MV) weights are applied to the ultrasonic echoes and the final image is obtained by DMAS. The results show the effectiveness of the proposed method in achieving a significant improvement of contrast resolution. Matrone et al. [19] proposed Filtered-Delay Multiply And Sum (F-DMAS), which can provide further improvements in image quality than DMAS. Luo et al. [20] proposed a wedge two-layer medium ultrasonic plane wave compound imaging method based on Sign Multiply Coherence Factor weighted DMAS beamforming to improve image quality further. The DMAS algorithm can improve signal coherence by performing a large number of autocorrelation combination multiplications, making the image computation significantly time-consuming, so it's limited for some industrial applications.

Alternatively, a sparse array optimization method provides an effective solution to some of these shortcomings. A few elements from the array are selected for transmission, while all or just some are used for reception, reducing the acquisition time and the amount of data to be processed. Bannouf et al. [21] proposed an algorithm based on optimization of the PSF to the design of sparse array. The results show that the number of elements can be reduced by at least 4 without great loss of image quality compared to full array imaging. Piedade et al. [22] proposed a sparse array approach to increase TFM productivity by reducing the number of transmission elements. The results show that the proposed sparse TFM can increase TFM productivity without compromising the CNR and API levels. Zhu et al. [23] proposed a discrete slime mold algorithm to optimization a sparse array. A fitness function with a narrow main-lobe and low side-lobe was constructed to obtain the sparse array position with the best performance, and the proposed method can reduce time consumption and improve the imaging efficiency.

In addition to the above methods of improving imaging efficiency by compressing data volume, many researchers have used hardware devices to accelerate algorithm implementation. Romero-Laorden et al. [24] presented different parallelization strategies for multicore CPU and GPU architectures in synthetic aperture ultrasonic imaging applications. Njiki et al. [25] proposed a multi-FPGA architecture consisting of a V5FX70T Xilinx Field Programmable Gate Array (FPGA) for controlling and processing high-level tasks and four V5SX95T Xilinx FPGAs for collecting and processing low-level tasks to reduce the execution time of FMC-TFM, effectively reducing the imaging time.

In this study, a Parallel Sparse Delay Multiply and Sum (PSDMAS) imaging algorithm based on DMAS and Graphics Processing Unit (GPU) is proposed. This algorithm exploits the spatial coherence of FMC data to overcome the shortcomings of TFM algorithms, which only use time-domain information of the ultrasound signal. To address the computational complexity of the DMAS focusing imaging algorithm, a genetic algorithm is used to perform sparse processing on the array to reduce the volume of data. The region of interest (ROI) is then imaged using parallel computation on the GPU to improve imaging efficiency. Experimental results show that this method can achieve detection capabilities similar to DMAS without increasing the time complexity of the algorithm.

2 Delay multiply and sum focusing imaging method

2.1 Full matrix capture

The FMC acquisition principle is shown in Fig.1, where each element of the phased array is excited sequentially and all elements receive the echo signal, which is labeled as S_{ij}, where i=1,2,...,N, j=1,2,...,N. i represents the transmitting element, j represents the receiving element. Once all the signals have been collected, a data set consisting of $N\times N$ ultrasound signals is obtained, i.e., the full matrix dataset. Due to the completeness of its data, it is widely used in various phased array imaging algorithms [3].

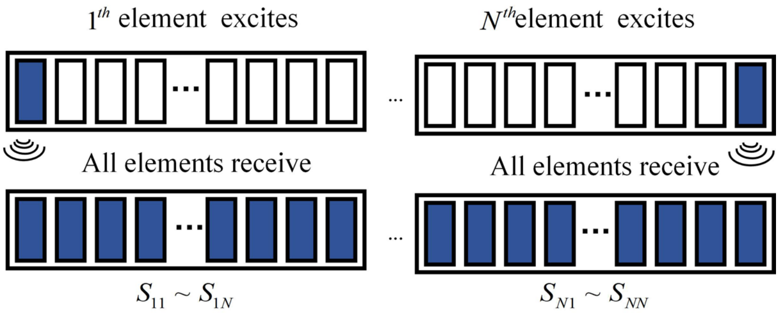

Fig. 1. Principle of full matrix capture

2.2 The principle of DMAS

In traditional ultrasonic phased array imaging algorithms such as TFM, the beamforming process often employs DAS. Firstly, the acoustic travel time from the virtual focal point to each corresponding array element is accurately calculated. Then, the acoustic acoustic pressure amplitude is extracted from the received ultrasound signal based on the acoustic travel time. Finally, the extracted amplitude values are accumulated to construct the final ultrasound image. The imaging algorithms only utilize the amplitude information of the ultrasound signals, but ignore the spatial coherence information of the signals. DMAS is a beamforming algorithm based on spatial coherence, which can improve the poor anti-interference ability of the DAS and enhance the lateral resolution and contrast of the image. Taking the ultrasonic signal received by N elements as an example, the implementation principle of the DMAS beamforming algorithm is shown in Fig.2.

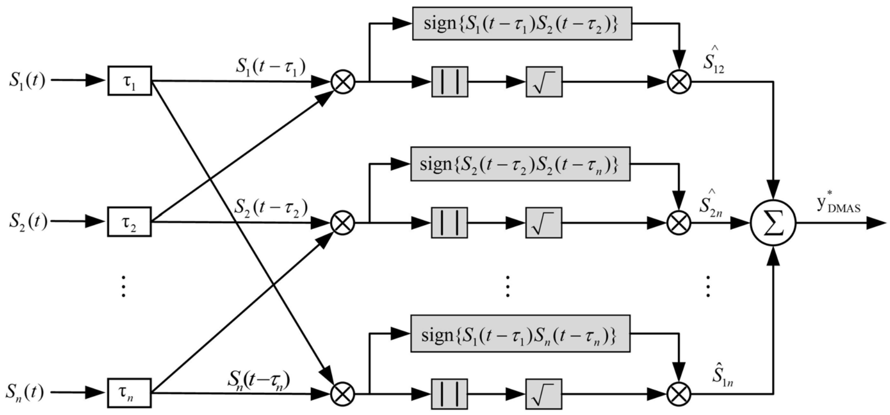

Fig. 2. Principle of DMAS beamforming algorithm

Firstly, similar to the DAS algorithm, the received echo signal is delayed to produce the delayed signal, denoted as $S_j(t\text{-}\tau_j)$, where n is the index of the receiving element, ranging from 1 to N, τ_j is the time-of-flight of the j-th received signal can be expressed as,

$$\tau_j = \frac{\sqrt{(y-y_j)^2-(\mathrm{z}\text{-}\mathrm{z}_j)^2}}{c_s} - \frac{z}{c_s} \tag{1}$$

where (y,z) is the coordinates of the virtual focusing point, (y_j,z_j) is the coordinates of the center point of the receiving element j.

Then, for each i and j, the delayed ultrasonic signals are multiplied by their absolute values to perform the combination multiplication. The square root of the resulting product is then calculated. Finally, the resulting value is multiplied by the sign function of the product of the two signals to obtain a new output signal $\hat{S}_{ij}$:

$$\hat{S}_{ij} = \mathrm{sign}\{s_i(t-\tau_\mathrm{i})s_j(t-\tau_j)\}\sqrt{|s_i(t-\tau_\mathrm{i})||s_j(t-\tau_j)|} \tag{2}$$

where sign( ) is a sign function which ensures that the polarity of the signal remains unchanged after multiplication.

Finally, the new set of beamforming signal are obtained as:

$$Y^*_{DMAS}(t) = \sum_{i=1}^{N-1}\sum_{j=i+1}^{N}\hat{S}_{ij} \tag{3}$$

where N is the number of array elements. As shown in Fig.3, the imaging area is defined according to the detection area, and each pixel in the imaging area is considered as a virtual focusing point. The expression for the pressure amplitude of the virtual focusing point when emitted by element i and received by element j is:

$$I_{ij}(y,z) = \sum_{j=1}^{j=N-1}\hat{S}_{ij}\sum_{k=j+1}^{k=N}\hat{S}_{ik} = \sum_{j=1}^{j=N-1}S_{ij}(t(y,z))\sum_{k=j+1}^{N}S_{ik}(t-\tau) \tag{4}$$

where $t(y,z)$ is the time delay between the focusing point and the transmitting and receiving elements, with

$$t(y,z) = \frac{\sqrt{(y_i-y)^2+z_i^2}+\sqrt{(y_j-y)^2+z_j^2}}{c_s} \tag{5}$$

(y_i, z_i) is the coordinates of the transmitting element.

According to Eq. (4), the DMAS focus algorithm expression based on the full matrix dataset can be derived as:

$$I(y,z) = \sum_{i=1}^{i=N} \sum_{j=1}^{j=N-1} I_{ij}(y,z) \tag{6}$$

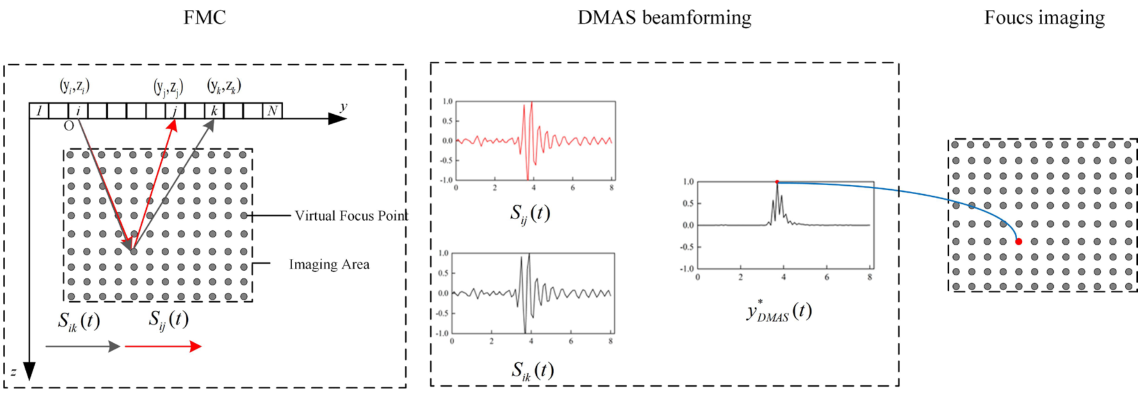

Fig. 3. Principle of DMAS focusing imaging

2.3 Imaging quantify factor

In UPA testing, the Array Performance Indicator (API) is used as an evaluation criterion for the imaging quality [13]. The API is calculated based on the image value of the point reflector detection and imaging ability. The API is defined as

$$API = \frac{A_{-6\mathrm{dB}}}{\lambda^2} \tag{7}$$

where $A_{-6\mathrm{dB}}$ is the area of the imaging region when the signal amplitude decreases by 6dB relative to the maximum value, λ is the wavelength of the ultrasonic wave in the detected workpiece. The smaller the API value, the better the resolution of the imaging system.

To quantitatively analysis the defect location results, the defect positioning error is defined as the relative distance between the position of the defect on the test sample and on the image. The highest point coordinate of the image amplitude at the defect location is taken as the center position of the detected defect. The smaller the difference, the better the positioning accuracy.

3 Sparse array optimization

3.1 Design of sparse array

In this paper, sparse processing is performed on the array elements, and the effective array is set to $N/2$. Matrix data of the sparse array is collected for DMAS focusing imaging. The sparse arrangement of array elements can be designed based on the effective aperture of the full array [27], so that the sparse array and the full array have similar effective apertures. In the sparse array, the effective array elements are randomly arranged within the aperture range, and the array's directional pattern is closely related to the element arrangement. It is difficult to use an analytical solution to find the optimal solution for the array arrangement. This paper uses a genetic algorithm to obtain the optimal solution, the sparse array optimization process is shown in Fig.4. The directional pattern function of a linear array is [28]:

$$F(\theta)=\sum_{m=1}^{N} e^{j\frac{2\pi}{\lambda}d_m(\sin\theta-\sin\theta_0)}\cdot f_m \tag{8}$$

where d_m is the position of the m-th array element relative to the first array element, θ is the angle between the incident wave and the normal of the linear array, and θ_0 is the direction angle of the linear array. f_m is the element state vector, where the elements state is 0 or 1, and $f_m=1$ represent the working state of element m and $f_m=0$ for the non-working state.

The maximum side-lobe of the acoustic field of the sparse array is:

$$S_{\max sll}=\max_{\phi\in S}\{F_{dB}(\theta)\}=\max_{\phi\in S}\left\{\left|\frac{F(\theta)}{\max(F(\theta))}\right|\right\} \tag{9}$$

where $F_{dB}(\theta)$ is the normalized array directional pattern, and S is the side-lobe region of the array directional pattern. According to Equation (10), if the zero-power point of the main lobe in the directional pattern is $2\varphi_0$, then the side-lobe region can be written as:

$$S = \{\theta \mid \theta_{\min} \le \theta \le \theta_0 - \varphi_0 \cup \theta_0 + \varphi_0 \le \theta \le \theta_{\max}\} \tag{10}$$

The optimization model can be defined as follows:

$$\min_f (S_{\max sll}) \tag{11}$$

where min( ) is the minimum value function, and the variable f is used to optimize the sparse layout of the linear array, so that the maximum side-lobe level $S_{\max sll}$ of the directional pattern of sparse linear array is minimized.

The peak side-lobe ratio for sparse arrays is [29]:

$$PSLR = 10\log_{10}(\frac{S_{\max sll}}{I_m}) \tag{12}$$

where I_m is the strength of the main-lobe.

Flowchart of sparse array optimization is shown in Fig. 4.

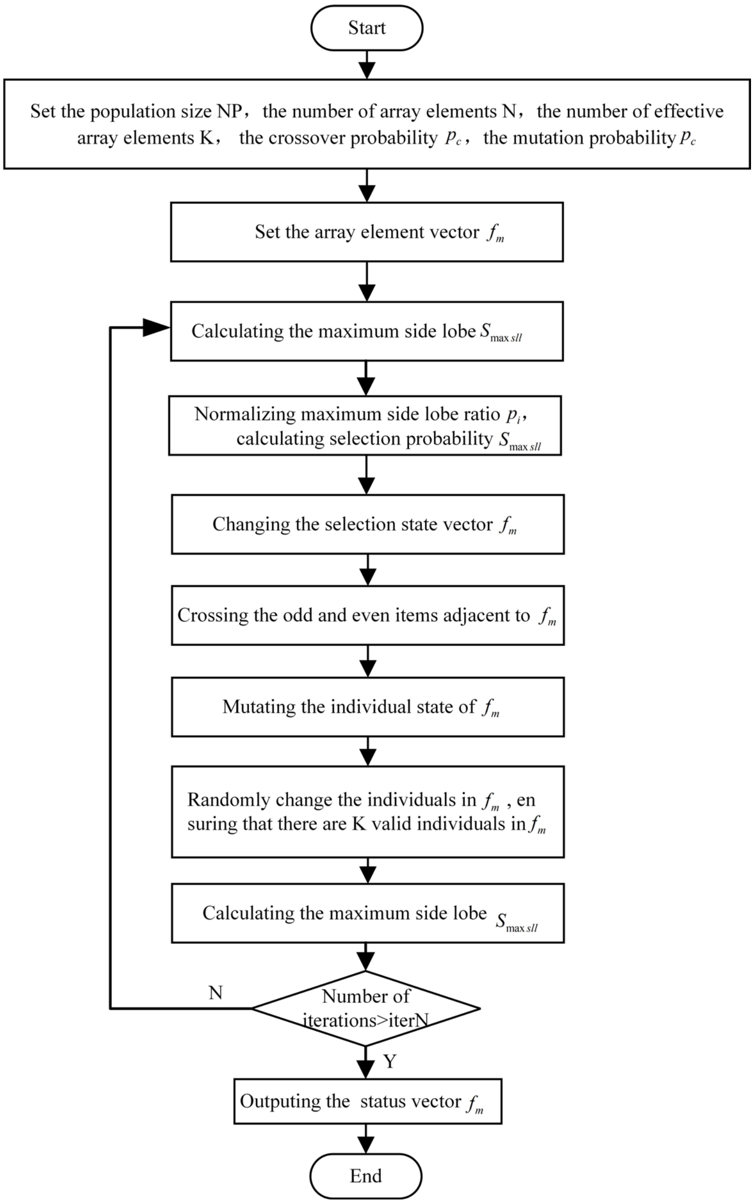

Fig. 4. Flowchart of sparse array optimization

3.2 Time complexity

In TFM, the DAS is used to produce a focused image with better resolution than a conventional phased array image. The amplitude of pixel is obtained by accumulating N^2 ultrasonic signals, The TFM cost for P image points is $O(N^2 \times P)$ [26]. When using the DMAS focusing imaging algorithm, the amplitude of a virtual focusing point needs to be calculated by summing the pressure amplitudes of $N^2(N-1)/2$ ultrasonic signals.

the delayed ultrasonic signals are multiplied by their absolute values to perform the combination multiplication. The square root of the resulting product is then calculated, the time complexity of the DMAS for P image points is $O(N^4(N-1)^2 \times P/4)$. While the DMAS focusing imaging algorithm can provide higher lateral contrast than TFM, the increased time complexity of the algorithm leads to a decrease in algorithm efficiency. The sparse arrangement of array elements is designed, when the effective array is set to $N/2$ „ the time complexity of the sparse DMAS for P image points is $O(N^4(N-2)^2 \times P/128)$.

4 Simulation and results

4.1 Simulation setup

Simulations were carried out using the FIELD II simulation programme in Matlab to evaluate the performance of the proposed method [17]. Schematic diagram of simulation is shown in Fig.5, the center of the first element is taken as the origin O, the array direction is the Y-axis, the depth direction is the Z-axis. The simulation scenario consists of ten 0.2mm diameter targets at five different depths placed at the center of the imaging area, and each target consisting of 5000 scatters with a reflection coefficient of 1. The two adjacent targets are separated by 4 mm in the y-direction and 2 mm in the z-direction, respectively. From top to bottom, the targets on the left are numbered 1-5, and those on the right are numbered 6-10.

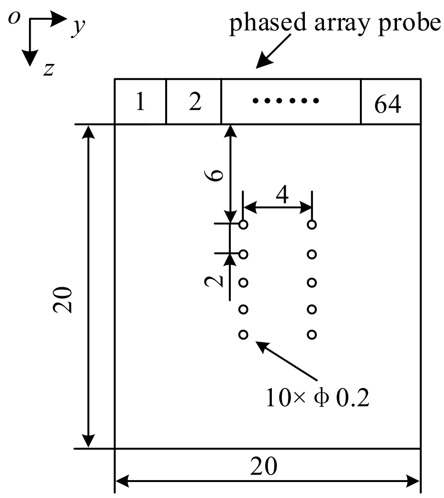

Fig. 5. Schematic diagram of simulation

A linear array transducer with 64 elements was simulated to act as both transmitter and receiver, the pitch of the element is 0.1mm, the width and length of the element are 0.4mm and 12mm, respectively. The center frequency of the transducer is 5 MHz. The transmitted pulse was a Gaussian-windowed 3-cycle sinusoidal burst at 5 MHz and the simulations were based on a homogeneous propagation medium with a sound speed set to 5900 m/s.

The full matrix data collected was imaged using SAFT, TFM, and DMAS, the imaging area in both Y-axis and Z-axis is 0~20mm, with a pixel point interval of 0.1mm. The performance of the algorithms was tested on a personal computer with an I5-7300hq CPU and NVIDIA GTX 1050 GPU, operating system version Windows 10, 16 GB of memory, and MATLAB version 2020B. The results are shown in Fig.6, Fig. 6(a) is the image reconstructed by SAFT, it has strong background speckle and artifacts, it is difficult to identify defects in the low resolution image. Fig. 6(b) is the image reconstructed by TFM, the contour of the targets was restored, the area of artifacts was significantly reduced and only a few artifacts were distributed around the targets. Fig. 6(c) is the image reconstructed by DMAS, the contour of the targets was clearly restored, the noise and artifacts were almost fully suppressed.

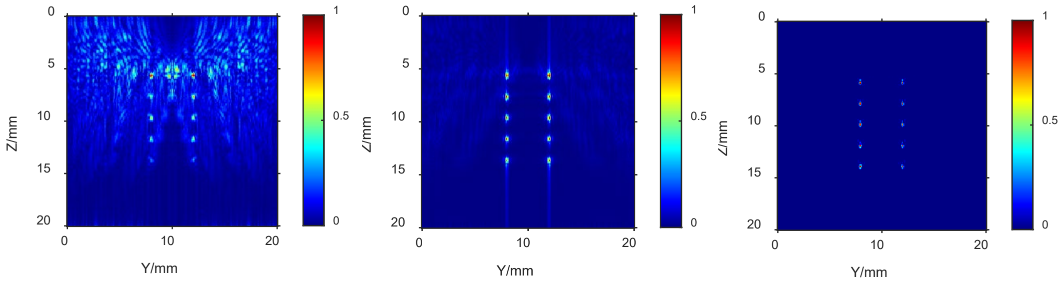

(a) (b) (c)

Fig. 6 Imaging results of (a)SAFT, (b)TFM and (c)DMAS

The API value of the defect is calculated by the Eq. (7), the result was shown in Fig.7. SAFT has the highest average API and the worst image resolution. DMAS has a significantly lower average API than SAFT and TFM and the best image resolution. In terms of defect positioning error, DMAS has the lowest average positioning error and the best positioning capability.

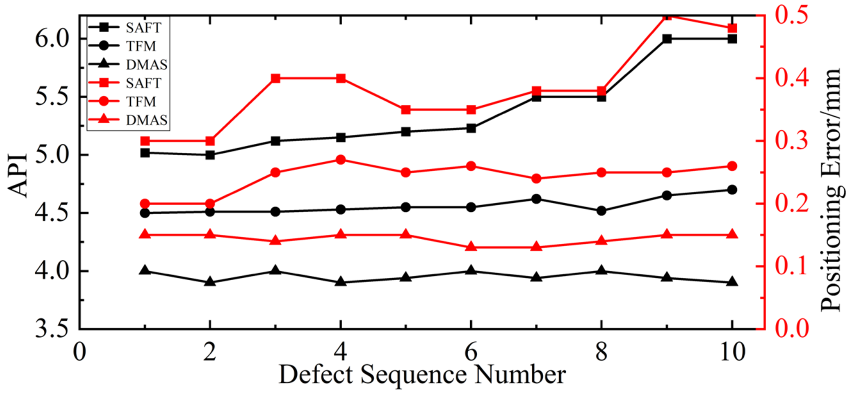

Fig. 7. Imaging quality comparison of SAFT, TFM and DMAS.

The transverse sound pressure intensity distribution at the Z=6mm were shown in Fig.8, The main-lobe of the DMAS algorithm is narrower than that of TFM, and the peak of the main-lobe is closer to the defect center, confirming that DMAS is superior to TFM in terms of defect location and quantitative indicators. In terms of side-lobe amplitude, the side-lobe of SAFT imaging is the highest, especially with large peak fluctuations between the two defects, indicating that the side-lobe suppression effect of SAFT is poor, resulting in poor image lateral contrast and resolution. When TFM is used for focusing imaging, the side-lobe suppression between defects is better than SAFT, but there is still significant side-lobe fluctuation on both sides of the defect, resulting in significant lateral side-lobe and low resolution.

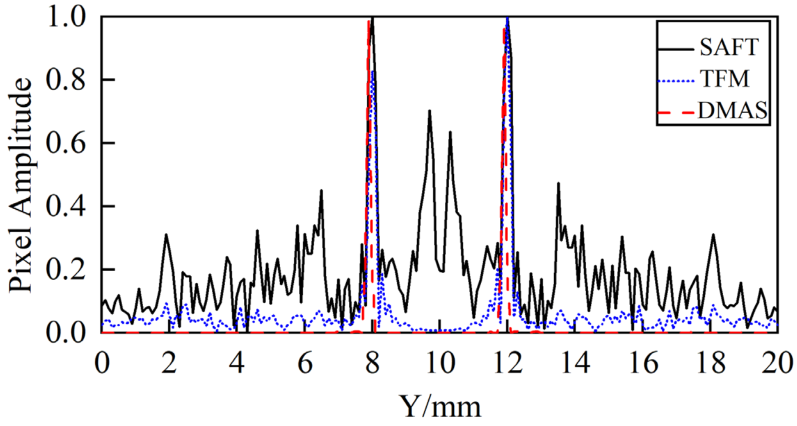

Fig. 8. The transverse sound pressure intensity at Z=6mm

When DMAS is used to reconstruct the image, its amplitude at non-defective pixels in the lateral direction is significantly smaller than that of SAFT and TFM, and the side-lobe suppression is evident. The imaging times for the SAFT, TFM and DMAS algorithms are 0.17 seconds, 5 seconds and 5640 seconds respectively. The calculation time for DMAS is 1128 times that TFM.

4.2 Sparse Array Designing and parallel computing

Based on the principle of the array pattern, under the premise of the same effective aperture of the array elements, the genetic algorithm is used to control the main-lobe width and side-lobe amplitude, which reflect the detection effect of the array in the array pattern, and to solve the optimal arrangement of the sparse array, thereby achieving a balance between the imaging effect and the data volume, and improving the imaging efficiency.

The initial population is large, the algorithm has a long convergence time and the results may not be optimized. Too few iterations will result in poor convergence of the algorithm, too many iterations will result in premature convergence of the algorithm. Although a higher crossover probability can speed up convergence, it can cause the algorithm to enter local optima too early. The crossover probability is small and the algorithm cannot escape from local optima. Although a higher mutation probability can maintain population diversity and help escape local optima, too high a mutation probability can also affect the convergence speed and stability of the algorithm. Based on the commonly used parameter value range and extensive experimental validation, the initial population size is 40, the iteration number is 200, the crossover probability is 0.5, and the mutation probability is 0.01.

The array element arrangement after sparse processing using genetic algorithm is 1000 0000 0010 0000 1101 0111 1111 1111 1111 1111 1110 1011 0000 0100 0000 0001, where 1 represents that the element is working at that position, and 0 represents that the element is not working at that position. Fig.9(a) is the Full array acoustic field pattern, and Fig.9(b) is the Sparse array acoustic field pattern. The main-lobes of both arrays are concentrated around 5º. According to Eq. (12), the peak side-lobe ratio of the sparse array is $PSLR = -16.25dB$, which meets the detection requirements [24].

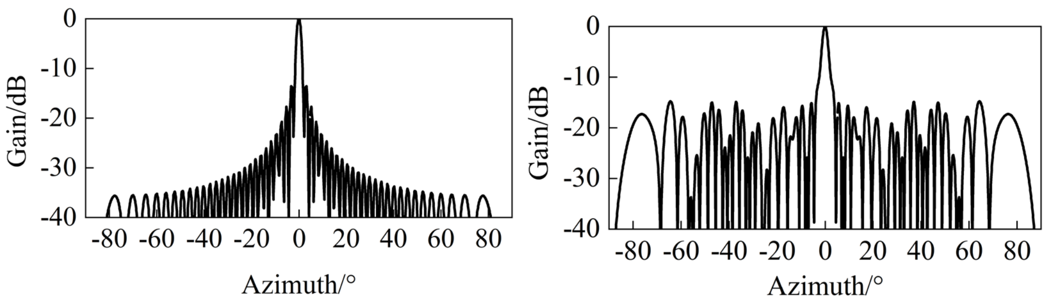

(a) (b)

Fig. 9. Diagram of acoustic field pattern (a) Full array, and (b) Sparse array.

Based on the sparse array state vector f_m, the working status of the array elements is set while other simulation parameters remain unchanged. The data of the full matrix is reduced from 64x64 to 32x32, resulting in a significant reduction in data volume.

The proposed PSDMAS image algorithm is implemented on the NVIDIA GTX 1050 produced by NVIDIA Corporation, the core code of the GTX1050 is GP107-300, which has 640 stream processors, 32 raster units, 40 texture units, and a core base frequency of 1354 MHz. It is equipped with 2GB of GDDR5 memory, the CUDA pseudocode of which is shown in Table 1.

Tab.1 The CUDA's pseudocode of PSDMAS

Algorithm:PSDMAS

```
int i = blockIdx.x * blockDim.x + threadIdx.x;
for (int j = 0; j < fmcPara->element * fmcPara->element-1; ++j)
        float times = (float)len / fmcPara->speed;
        a=fmcMat[j*fmcPara->signalLen+(int)(times * fmcPara->sampleFre)];
        for (int k= j+1; k < fmcPara->element * fmcPara->element-1; ++k)
                float times1 = (float)len1 / fmcPara->speed;
                b = fmcMat[k*fmcPara->signalLen+(int)(times1 * fmcPara->sampleFre)];
                product = sqrt(fabs(a * b));
                product = copysign(product, a * b);
                imgMat[i] += product;
```

The sparse 32x32 matrix dataset are then imaged using PSDMAS, the PSDMAS image is compared with the DMAS image obtained using full matrix phased array configurations. As shown in Fig.10, there are a few low-intensity artifacts around the targets in the image of PSDMAS, the image obtain using PSDMAS had a resolution close to that using DMAS.

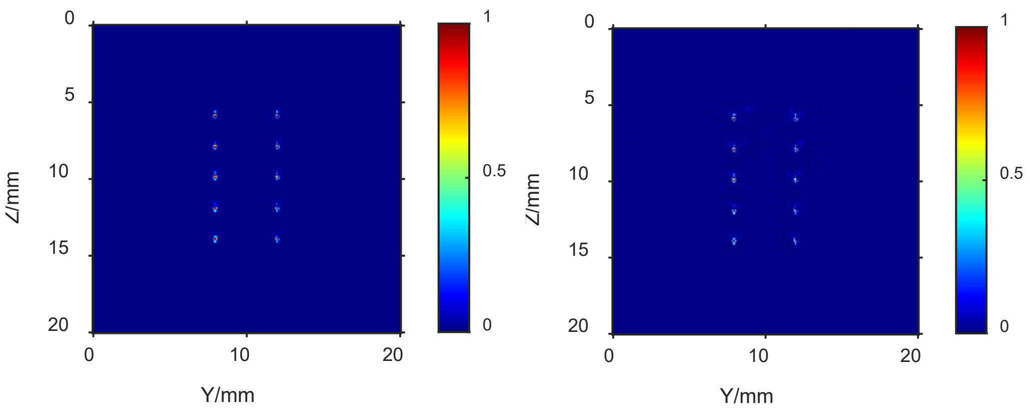

(a) (b)

Fig.10 Imaging results of (a) DMAS and (b) PSDMAS.

The API and positioning errors from Fig. 10 are calculated and shown in Fig. 11, the API average values of DMAS and PSDMAS is 3.9 and 4.2, respectively. The positioning error of DMAS and DMAS is 0.15mm and 0.21mm, respectively. The difference between

API and positioning errors are 0.3 and 0.06mm, respectively. The results indicates that PSDMAS and DMAS have similar defect detection capabilities.

The transverse sound pressure intensity distribution at the Z=6mm is shown in Fig.12, the main-lobes of both DMAS and PSDMAS algorithms are narrower and the peak of the main-lobe is closer to the defect center, confirming that both algorithms are able to accurately locate defects. In summary, the lateral resolutions of PSDMAS and DMAS are similar and significantly better than TFM. The obtained results demonstrate that the sparse matrix phased array configurations can provide high imaging performance and efficiency.

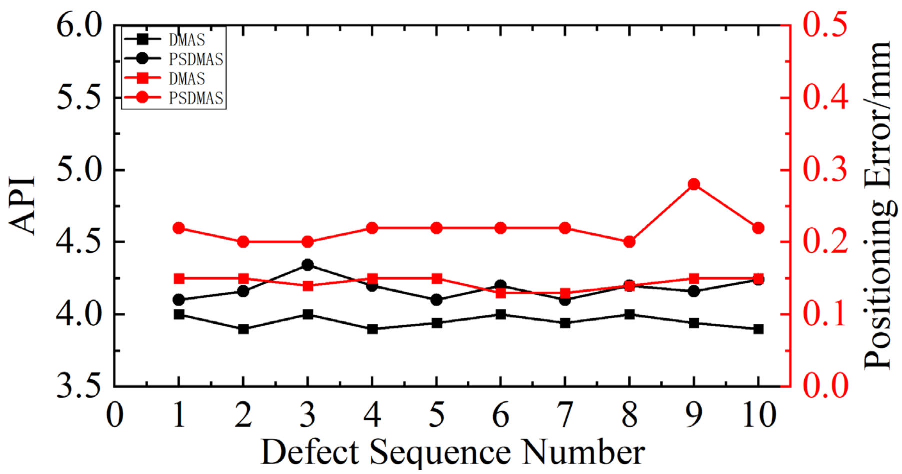

Fig.11 Imaging quality comparison of DMAS and PSDMAS

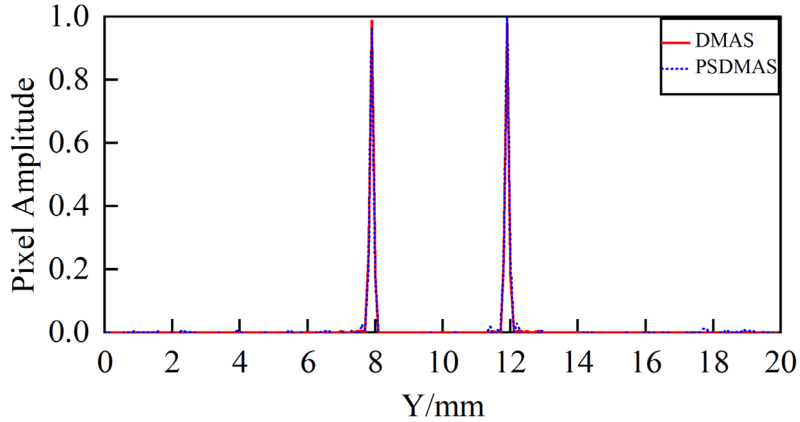

Fig.12 The transverse sound pressure intensity at Z=6mm

The DMAS and PSDMAS algorithms are operated 5 times respectively, taking the total average to reduce errors, the results are shown in Tab. 2, the run times for the DMAS and PSDMAS algorithms are 5639 seconds and 5.97 seconds, respectively. The run time of PSDMAS is reduced by 99.9% compared to DMAS.

Tab.2 Total run time of TFM, DMAS and PSDMAS

Imaging method	Total run time / s					
	1	2	3	4	5	Mean
DMAS	5640	5646	5630	5641	5642	5639
PSDMAS	5.95	5.99	5.95	5.97	5.96	5.97

5 Experimental and results

Experiments were further performed to evaluate the proposed method in practice. As shown in Fig.13, the FMC dataset was acquired using a Verasonics Vantage-64 ultrasound phased array system (Verasonics Inc., Kirkland, WA, USA), a 64-element Imasonic linear array (Imasonic Inc., Besanson, France) with a center frequencies of 5 MHz was used, the pitch of the element is 0.1mm, the width and length of the element are 0.4mm and 12mm, respectively. A steel test block with a series of through holes was used as the imaging object. The specific details of the through holes and the imaging area of the experiments are shown in Fig. 13(b), the targets are numbered 1-5 from left to right. The parameters of the experimental system were kept consistent with the simulation setup.

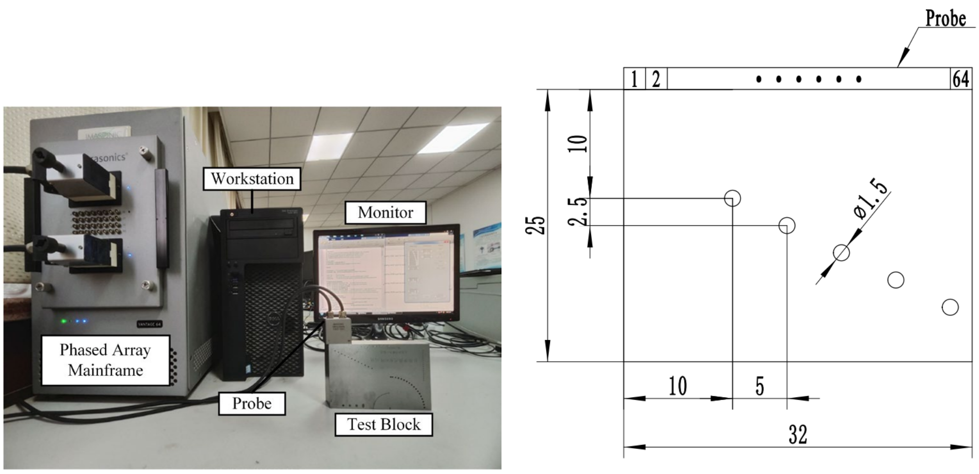

(a) (b)

Fig.13 The experimental configuration. (a) Phased array platform (b) ROI imaging area

Adjusting the probe position, making the center of the first element to the leftmost side of the test block, as shown in Fig.13(b). The imaging area in the Y-axis is 0~35mm, and the imaging area in the Z-axis is 0~25mm, with a pixel point interval of 0.1mm. The imaging results of test block were shown in Fig.14. Fig. 14(a) is the image reconstructed by TFM, the contour of the targets was restored, the area of artifacts was reduced. Fig. 14(b) and Fig. 14(c) are the image reconstructed by DMAS and PSDMAS, respectively, the contour of the targets was clearly restored, the noise and artifacts were almost fully suppressed.

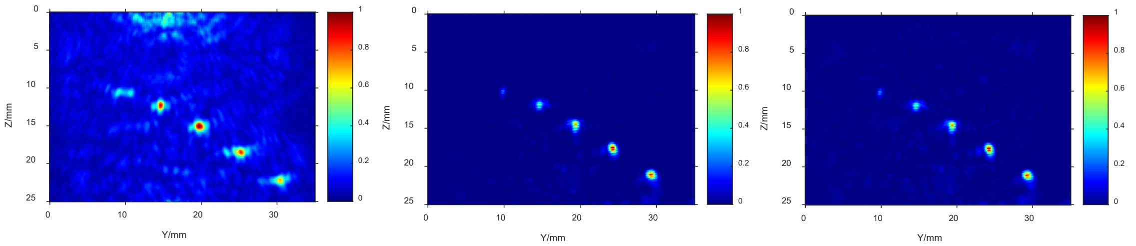

(a) (b) (c)

Fig.14 Imaging results of (a) TFM, (b) DMAS and (c) PSDMAS.

The API and position errors from Fig. 14 are calculated and shown in Fig. 15, DMAS and PSDMAS provided a considerable improvement in API and positioning error compared with TFM, the image contrast of the DMAS and PSDMAS imaging algorithms is significantly better than TFM. For the defect number 1 with z=10mm, the pixel amplitude is low and the range at the defect location is small, the API is much larger than other defects, it is easily misjudged as an artefact, resulting in missed detection.

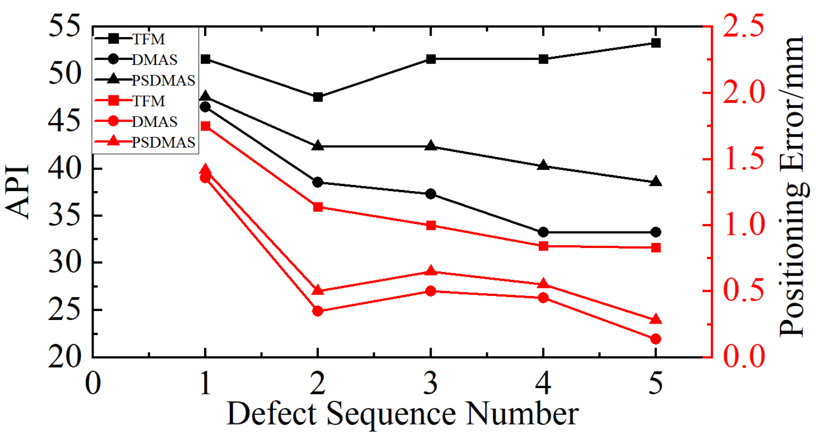

Fig.15 Imaging quality comparison of TFM, DMAS and PSDMAS.

The transverse sound pressure intensity distribution for all targets were shown in Fig.16, the main-lobes of both DMAS and PSDMAS algorithms are narrower and the peak of the main-lobe is closer to the defect center, the lateral resolutions of PSDMAS and DMAS are similar and significantly better than TFM.

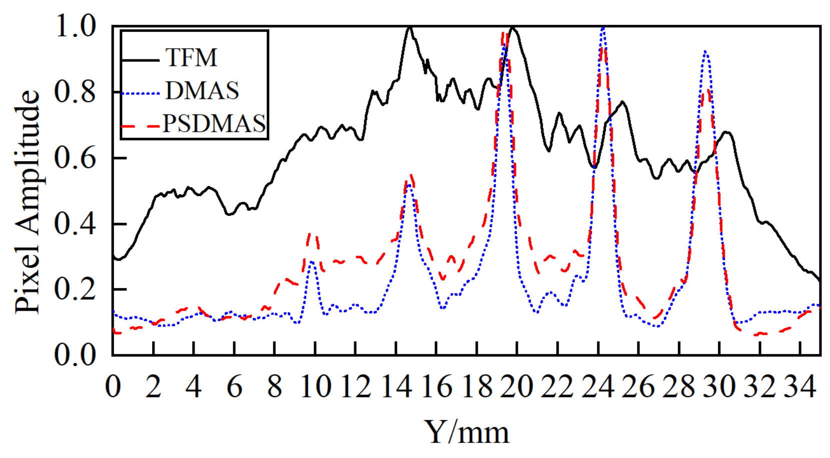

Fig. 16 The transverse sound pressure intensity for all targets.

The position error and API values of PSDMAS and DMAS are similar, and the detection ability of the two algorithms is similar. The computation time cost of DMAS is about 7550 seconds, while that of the PSDMAS method proposed in this paper is only 7.21 seconds. The computation time of PSDMAS was reduced by 99.9% compared to DMAS, and the imaging efficiency was significantly improved.

6 Conclusion

In this study, we proposed an optimized Delay Multiply and Sum method to reduce time consumption and improve the imaging solution. DMAS utilize the spatial coherence information of the ultrasound signals, which can improve the poor anti-interference ability of the DAS and enhance the lateral resolution and contrast of the image. A comparative study between TFM and DMAS was conducted in terms of API value and defect positioning error, and DMAS could enhance the spatial coherence and suppress the clutter artifacts, however, the time complexity of the DMAS algorithm increases from $O(N^2 \times P)$ to $O(N^4(N-1)^2 \times P/4)$ than TFM, the imaging time of DMAS is about 1100 times longer than TFM. A sparse array optimization method is applied to reduce the amount of data. A fitness function with ratio of main-lobe width and side-lobe peak was constructed, the sparse array position with the best performance could obtain using a genetic algorithm, when the effective array is set to $N/2$, and the data of the full matrix is reduced from N^2 to $N^2/4$, the time complexity of the sparse DMAS for P image points is $O(N^4(N-2)^2 \times P/128)$. The parallel architecture of the GPU is then used to accelerate the algorithm. Both DMAS and PSDMAS have similar side-lobe suppression capabilities, and the computation time of PSDMAS is reduced by 99.9% compared to DMAS. The imaging efficiency is significantly improved, achieving a good balance between image resolution and algorithm efficiency. For defects in the near-field region, the pixel amplitude is low and the range at the defect location is small, their image resolution and contrast are still poor, the API is much larger than other defects, it is easyly misjudged as an artefact, resulting in missed detection.

PSDMAS offers a promising alternative solution for PAUT imaging in NDT with improved imaging performance. Future research will include the robustness of PSDMAS under different noise levels, defect types and material property variations to ensure that the algorithm can achieve the expected results in practical applications.

Competing interests: All authors declare that we have no any competing interests as defined by Springer, or other interests that might be perceived to influence the results and /or discussion reported in this paper.

Disclosure statement: No potential conflict of interest was reported by the author(s)

Funding :This work is supported by the National Natural Science Foundation of China [Grant Nos. 51705418, 52175518 and 52274158] and the Xi'an Science and Technology Plan Project [Grant No. 2024JH-GXFW-0207].

Reference

[1] Smoqi Z, Sotelo L D, Gaikwad A, et al. Ultrasonic nondestructive evaluation of additivel y manufactured wear coatings[J]. NDT & E International, 2023, 133: 102754. https://doi.org/10.1016/j.ndteint.2022.102754

[2] Ha J M, Seung H M, Choi W. Autoencoder-based detection of near-surface defects in ult

rasonic testing[J]. Ultrasonics, 2022, 119: 106637. https://doi.org/10.1016/j.ultras.2021.106637
[3] Zhao J, Yang K, Du X, et al. Automated quantification of small defects in ultrasonic phased array imaging using AWGA-gcForest algorithm. Nondestructive Testing and Evaluation, 2023: 1-22. https://doi.org/10.1080/10589759.2023.2274001.
[4] Li Y, Zhou Z, Wang J. Analysis of linear non-destructive testing and evaluation methods for thin-walled structure inspection using ultrasonic array. Coatings, 2019, 9(2): 146. https://doi.org/10.3390/coatings9020146.
[5] Zhang H, Chen S L, Jia L C. Three-dimensional total-focus imaging based on ultrasonic linear phased array. Journal of Electronic Measurement and Instrumentation，2016,30(7):992-999. https://doi.org/10.13382/j.jemi.2016.07.002.
[6] Wang T, Deng W, Wang H, et al. Automated ultrasonic testing for near-surface flaws in CFRP[J]. Nondestructive Testing and Evaluation, 2024: 1-20. https://doi.org/10.1080/10589759.2024.2337062.
[7] Ming D, Hui T, Hong-Wei M, et al. Acoustic field simulation-based ultrasonic water im mersion non-destructive testing for titanium alloy plate[J]. Nondestructive Testing and Evaluat ion, 2024: 1-14. https://doi.org/10.1080/10589759.2024.2306469
[8] Hwang Y I, Park J, Kim H J, et al. Performance comparison of ultrasonic focusing techniques for phased array ultrasonic inspection of dissimilar metal welds. International Journal of Precision Engineering and Manufacturing, 2019, 20: 525-534. https://doi.org/10.1007/s12541-019-00085-1.
[9] Mohammadkhani R, Zanotti Fragonara L, Padiyar M J, et al. Improving depth resolution of ultrasonic phased array imaging to inspect aerospace composite structures. Nature reviews Cancer, 2020, 20(2): 559. https://doi.org/10.3390/s20020559
[10] Ling K H, Fuh Y K, Kuo T C, et al. Effect of welding sequence of a multi-pass temper bead in gas-shielded flux-cored arc welding process: hardness, microstructure, and impact toughness analysis. The International Journal of Advanced Manufacturing Technology, 2015, 81: 1033-1046. https://doi.org/10.1007/s00170-015-7277-x
[11] Tian Z, Howden S, Ma Z, et al. Pulsed laser-scanning laser Doppler vibrometer (PL-SLDV) phased arrays for damage detection in aluminum plates. Mechanical systems and signal processing, 2019, 121: 158-170. https://doi.org/10.1016/j.ymssp.2018.11.016.
[12] Wang Y, Huang L, Wang R, et al. Improved ultrafast power Doppler imaging using united spatial-angular adaptive scaling wiener postfilter[J]. IEEE Transactions on Ultrasonics, Ferroelectrics, and Frequency Control, 2023, 70(9): 1118-1134. https:// doi:10.1109/TUFFC.2023.3297571
[13] Nanekar P, Kumar A, Jayakumar T. SAFT-assisted sound beam focusing using phased arrays (PA-SAFT) for non-destructive evaluation. Nondestructive Testing and Evaluation, 2015, 30(2): 105-123. https://doi.org/10.1080/10589759.2014.1002837.
[14] Madhavanunni A N, Panicker M R. Beam multiply and sum: A tradeoff between delay and sum and filtered delay multiply and sum beamforming for ultrafast ultrasound imaging. Biomedical Signal Processing and Control, 2023, 85: 104807. https://doi.org/10.1016/j.bspc.2023.104807.
[15] Lim H B, Nhung N T T, Li E P, et al. Confocal microwave imaging for breast cancer detection: Delay-multiply-and-sum image reconstruction algorithm. IEEE Transactions on Biomedical Engineering, 2008, 55(6): 1697-1704. https://doi.org/10.1109/TBME.2008.919716.
[16] Moubark A M, Alomari Z, Zaman M H M, et al. Optimizing the lateral beamforming step for

filtered-delay multiply and sum beamforming to improve active contour segmentation using ultrafast ultrasound imaging. Biomedical Signal Processing and Control, 2022, 71: 103267. https://doi.org/10.1016/j.bspc.2021.103267.
[17] Da T, Lishuai L, Yanxun X, Fu-Zhen X. An optimized total focusing method based on delay-multiply-and-sum for nondestructive testing. Ultrasonics, 2023, 128: 106881. https://doi.org/10.1016/j.ultras.2022.106881
[18] Ziksari MS, Asl BM. Minimum variance combined with modified delay multiply-and-sum beamforming for plane-wave compounding. IEEE Trans Ultrason Ferroelectrics Freq Control 2021;68:1641–1652. https://doi: 10.1109/TUFFC.2020.3043795.
[19] Matrone G，Savoia A S，Caliano G，Magenes G. Experimental evaluation of ultrasound higher-order harmonic imaging with Filtered-Delay Multiply And Sum (F-DMAS) non-linear beamforming. Ultrasonics, 2018,86:59-68. https://doi.org/10.1016/j.ultras.2018.01.002
[20] Luo L,Tan Y H, Li J L, Zhang Y, Gao X R. Wedge two-layer medium ultrasonic plane wave compounding imaging based on sign multiply coherence factor combined with delay multiply and sum beamforming. NDT & E International, 2022, 127: 102601. https://doi.org/10.1016/j.ndteint.2021.102601
[21] Bannouf S , Robert S , Casula O ,et al.Data set reduction for ultrasonic TFM imaging using the effective aperture approach and virtual sources. Journal of Physics Conference, 2013, 457(1):2007. DOI:10.1088/1742-6596/457/1/012007.
[22] Piedade L P , Painchaud-April G , Duff A L ,et al.Minimum transmission events for fast ultrasonic TFM imaging: A comparative study. NDT & E International, 2022, 128:102627. DOI:10.1016/j.ndteint.2022.102627.
[23] Zhu W F, Wei Z B, Xiang Y X, and et al. Minimum Variance Combined With Modified Delay Multiply-and-Sum Beamforming for Plane-Wave Compounding. IEEE Sensors Journal, 2024,24: 8. 12207 – 12216. DOI: 10.1109/JSEN.2024.3372579
[24] Romero-Laorden D, Villazón-Terrazas J, Martinez-Graullera O, et al. Analysis of parallel computing strategies to accelerate ultrasound imaging processes[J]. IEEE Transactions on Parallel and Distributed Systems, 2016, 27(12): 3429-3440.
[25] Njiki M, Elouardi A, Bouaziz S, et al. A multi-FPGA architecture-based real-time TFM ultrasound imaging[J]. Journal of Real-Time Image Processing, 2019, 16: 505-521.
[26] Cui W K, Qin K H. Total focusing method for ultrasonic non-destructive inspection of homogenous objects based on elliptical arc scan-conversion. Actta Electronica Sinica, 2017, 45(10):2375-2382. https://doi.org/10.3969/j.issn.0372-2112.2017.10.010.
[27] Lockwood G R, Li P C, O'Donnell M, et al. Optimizing the radiation pattern of sparse periodic linear arrays. IEEE Transactions on Ultrasonics, Ferroelectrics, and frequency control, 1996, 43(1): 7-14. https://doi.org/10.1109/58.484457.
[28] Zhang H, Zhu W F, Fan G P, et al. Thinned array ultrasonic imaging of debonding defects in discontinuous impedance bonded structures. Acta Physica Sinica， 2023,72(02):150-158.1. https://doi.org/10.7498/aps.72.20221771.
Wang W, LI C Y, Sun T ,et al. SAR image quality assessment of satellite TH-2-01. Acta Geodaetica et Cartographica Sinica,2022,51(12):2508-2516. https://doi.org/10.11947/j.AGCS.2022.20210420.